

# 1 Learned holographic light transport

2 KORAY KAVAKLI,<sup>1</sup> HAKAN UREY,<sup>1</sup> AND KAAN AKŞIT<sup>2,\*</sup>

3 <sup>1</sup>*Department of Electrical and Electronics Engineering, Koç University, Istanbul, Turkey*

4 <sup>2</sup>*Department of Computer Science, University College London, London, UK*

5 \*[k.aksit@ucl.ac.uk](mailto:k.aksit@ucl.ac.uk)

6 <https://kaanaksit.com>

7 **Abstract:** Computer-Generated Holography (CGH) algorithms often fall short in matching  
8 simulations with results from a physical holographic display. Our work addresses this mismatch  
9 by learning the holographic light transport in holographic displays. Using a camera and a  
10 holographic display, we capture the image reconstructions of optimized holograms that rely  
11 on ideal simulations to generate a dataset. Inspired by the ideal simulations, we learn a  
12 complex-valued convolution kernel that can propagate given holograms to captured photographs  
13 in our dataset. Our method can dramatically improve simulation accuracy and image quality in  
14 holographic displays while paving the way for physically informed learning approaches.

15 © 2021 Optical Society of America

## 16 1. Introduction

17 The future of human-computer interactions [1] demands technologies that can display life-  
18 like three-dimensional visuals. An emerging trend, Computer-Generated Holography (CGH),  
19 promises to deliver such realistic visuals in the next-generation displays [2]. However, CGH  
20 algorithms often fall short of achieving high image quality in real life.

21 The traditional CGH algorithms such as Gerchberg-Saxton method [3] or recently trending  
22 approaches such as Stochastic Gradient (SGD) based differentiable methods [4–6] can deliver an  
23 outstanding image quality in the simulation environments. However, in an actual holographic  
24 display with phase-only modulation, holograms optimized or learned using these ideal holographic  
25 light transport models often fail to deliver the same image quality. Identifying causes of mismatch  
26 and bridging the gap between the image qualities of simulations and actual experiments are  
27 growing scientific research trends in the holography community.

28 The traditional solutions [7] to address the mismatch aims to find complex residual values that  
29 can be added as a regularization term to the ideal holographic light transport [6] or the complex  
30 hologram [5]. These techniques to regularize holographic image reconstruction models [5, 6]  
31 are powerful and effective in practice. In the meantime, researchers have also garnered interest  
32 to learn the hologram generation process using deep learning [5, 8]. However, their proposed  
33 solutions often yield highly complex algorithmic structures and sometimes require a physically  
34 demanding experimentation routine. These complex algorithmic structures involve learning  
35 components such as Generative Adversarial Networks (GANs) that are not straightforward in  
36 tuning and training [6], multi-layer perceptrons that model the nonlinear response of an SLM,  
37 which may carry lesser semantic meaning for an optical scientist [5] or characterizing aberrations  
38 with Zernike polynomials that requires careful experimentation [5, 9–12]. We ask ourselves if the  
39 demand in experimentation load and complex nature of algorithms can be avoided while optical  
40 scientists can get more hints towards understanding imperfections in actual holographic displays.  
41 With that question in mind, we aim for deriving a new and refined CGH algorithm to improve  
42 image quality in actual holographic displays.

43 This work argues that a tailored holographic light transport model for a target holographic  
44 display can account for optical aberrations and bridge the gap between simulations and actual  
45 holographic displays. We also argue that such a model can avoid intensive experimentation

46 requirements in display calibration. For this purpose, we propose to learn a single complex-valued  
 47 point spread function that helps us to propagate input phase-only holograms to the target image  
 48 plane. Thus, our holographic light transport model convolves an input phase-only hologram  
 49 with a learned complex-valued point spread function to get to the physically accurate image  
 50 reconstructions in simulations for a target holographic display. The learning process involves  
 51 comparing image reconstruction in simulations against experiments using a camera with an  
 52 actual holographic display. Like any other learning process, we must have a set of data composed  
 53 of input phase-only holograms and their corresponding image reconstructions in an actual  
 54 holographic display. We collect such a dataset from our proof-of-concept display prototype using  
 55 a camera and an ideal holographic light transport based hologram optimization method that is fully  
 56 differentiable. We show that our learned holographic light transport can dramatically improve  
 57 simulation accuracy and final image quality in our holographic display. Our key contributions  
 58 are summarized as follows:

- 59 • Learned holographic light transport. We propose a learned approach for *holographic light*  
 60 *transport* to bridge the gap between simulations and experimentation. Our method learns  
 61 a single complex convolutional kernel to reconstruct images in simulation similar to the  
 62 real experiments. Our implementation is fully differentiable. We show that image quality  
 63 results from an actual holographic display can be enhanced with our method while the  
 64 simulations become highly accurate.
- 65 • Holographic dataset from a proof-of-concept holographic display. In order to be able to  
 66 train and derive a single complex convolutional kernel, we build a phase-only holographic  
 67 display. Then, we capture a series of photographs of holographic image reconstructions  
 68 resulting from holograms optimized using the ideal holographic light transport.

69 In the following sections, we will first introduce a standard ideal holographic light transport  
 70 model. Then, we will provide the details of our experimental setup. Finally, we will introduce our  
 71 technique in learning and provide quantitative results of our method while comparing it against  
 72 the ideal case.

## 73 2. Optimizing holograms with ideal holographic light transport

74 The topic of light transport plays a crucial role in formulating the basis of various domains  
 75 including traditional computer graphics [13], architecture [14], biomedical imaging [15], non-  
 76 line-of-sight imaging [16], three-dimensional printing [17], visible light communications [18],  
 77 holographic recording [19], computational displays [20], eye prescription correction [21], eye-  
 78 gaze tracking [22], ophthalmology [23] and many more. Although we cover only display  
 79 technologies in this work, an accurate representation method of light transport can potentially  
 80 pave the way towards enhancements in many other highlighted applications.

81 Light transport models used in CGH bases on Rayleigh-Sommerfeld diffraction integrals [24].  
 82 This diffraction integral's first solution, the Huygens-Fresnel principle, is expressed as follows:

$$u(x, y) = \frac{1}{j\lambda} \iint u_0(x, y) \frac{e^{jkr}}{r} \cos(\theta) dx dy, \quad (1)$$

83 where resultant field,  $u(x, y)$ , is calculated by integrating over every point across hologram plane  
 84 in XY axes,  $u_0(x, y)$  represents the optical field in the hologram plane for every point across XY  
 85 axes,  $r$  represents the optical path between a selected point in hologram plane and a selected  
 86 point in target plane,  $\theta$  represents the angle between these points,  $k$  represents the wavenumber  
 87 ( $\frac{2\pi}{\lambda}$ ) and  $\lambda$  represents the wavelength of light. In this model, optical fields,  $u_0(x, y)$  and  $u(x, y)$ ,  
 88 are represented with a complex value,

$$u_0(x, y) = A(x, y)e^{j\phi(x, y)}, \quad (2)$$

89 where  $A$  represents the spatial distribution of amplitude and  $\phi$  represents the spatial distribution of  
 90 phase across a hologram plane. To simplify our description, we can express the Huygens-Fresnel  
 91 principle as a superposition of diverging spherical waves originating from a hologram [25].  
 92 Perhaps one can also think of the Huygens-Fresnel principle as stamping a complex point-spread  
 93 function on a target image plane for each point of a hologram while weighting each stamp with  
 94 its amplitude and phase from its origin.

95 Calculating Huygens-Fresnel approximation by visiting each point on a hologram one by one  
 96 would consume a large computation and power budget while being slow in processing. Common  
 97 approaches in the literature [26–28] dedicated to near fields (e.g., short distances like 10 cm or  
 98 half a meter) formulates this integral as a convolution operation with a single complex kernel.  
 99 Hence, the common approaches [29] can be expressed as

$$\begin{aligned} u(x, y) &= u_0(x, y) * h(x, y) \\ &= \mathcal{F}^{-1}(\mathcal{F}(u_0(x, y))\mathcal{F}(h(x, y))) \\ &= U_0(f_x, f_y)H(f_x, f_y), \end{aligned} \quad (3)$$

100 where  $h$  represents a spatially varying complex convolution kernel. The value of the complex  
 101 kernel,  $h$ , is typically expressed as

$$h(x, y) = \frac{e^{jkz}}{j\lambda z} e^{\frac{jk}{2z}(x^2+y^2)}, \quad (4)$$

102 where  $z$  represents the distance between a hologram plane and a target image plane. This ideal  
 103 model is implemented in a differentiable fashion (refer to [odak.learn.wave.classical L81-114](#)) in  
 104 our fundamental library for optical sciences [30]. The same library hosts differentiable models of  
 105 various light transport approximations (refer to [odak.learn.wave.classical L8-53](#)).

106 Now that we have established an ideal holographic light transport model as in Equation 3.  
 107 We can use this holographic light transport model as a forward model that propagates light  
 108 from a hologram to a target plane. As mentioned earlier, since this model is implemented in  
 109 code using a modern machine learning library, PyTorch [31], we take advantage of the fact that  
 110 modern machine learning libraries are capable of automatically differentiating provided functions.  
 111 Differentiation helps to calculate the complex gradient of our forward model’s error. In simple  
 112 terms, for each input phase-only hologram, the resulting image reconstruction can be calculated,  
 113 and the impact of changing phase values on image reconstruction can be precisely estimated  
 114 using gradients. This fact helps an optimizer to have meaningful modifications on phase values  
 115 of a phase-only hologram at the each optimization step.

116 In order to fully realize the described optimization, a loss function is required. For this purpose,  
 117 we define a loss function,  $L$ , using least squared error between a reconstructed image at a target  
 118 plane,  $u(x, y)$ , and a target image,  $t(x, y)$ ,

$$L = (u(x, y) - t(x, y))^2. \quad (5)$$

119 Note that the loss function described here is the simplest case, and we leave customization of  
 120 this loss function to meet the application’s demands as a future discussion. In addition to a loss  
 121 function, we would require an optimizer to optimize our phase-only holograms for various targets.  
 122 We choose to use a Stochastic Gradient Descent based optimization method [32, 33] with a  
 123 learning rate of 0.1. We ran our optimizer using our ideal forward model for 200 iterations at each  
 124 hologram calculation. Our hologram optimization method (refer to ) is distributed as a part of our  
 125 fundamental library for optical sciences [30]. We also provide examples at [odak.test.learn\\_sgd](#)  
 126 for using the optimization method within our library.

127 Using the described ideal holographic light transport and hologram optimization methodology,  
 128 we calculate phase-only holograms of target images from DIV2K dataset [34]. We resize images

129 in DIV2K dataset to 1920x1080 to match the size of our SLM. We also convert those images  
 130 to monochrome by taking an average across three color channels. Note that all these images at  
 131 DIV2K dataset are used only in training (finding the holographic light transport kernel, not in test  
 132 cases). The calculated image reconstructions perfectly matching the target images in simulations,  
 133 however they have to be tested against photographs captured from an actual holographic display.  
 134 Thus, we will explain how we build a proof-of-concept holographic display in the next section  
 135 before explaining our final methodology to improve visual quality and realism.

### 136 3. Proof-of-concept holographic display

137 We build a proof-of-concept holographic display to assess image quality of our hologram  
 138 optimization methods that uses ideal holographic light transport. We will introduce our learned  
 139 holographic light transport in the next section, we will also use the same proof-of-concept  
 140 holographic display to assess image quality of our methodology.

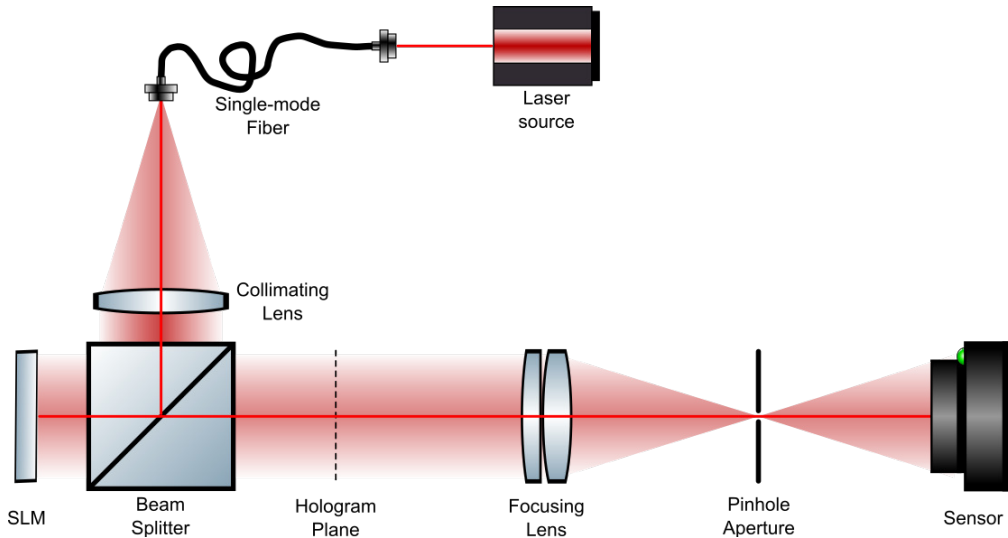


Fig. 1. Schematic diagram of our proof-of-concept holographic display prototype used in our experimental setup.

141 The optical layout of our proof-of-concept holographic display is represented in Figure 1.  
 142 Following the light from its source, the optical assembly of our proof-of-concept holographic  
 143 display uses a multi-wavelength laser light source, LASOS MCS4. However, for our experimentation,  
 144 we only rely on the working wavelength of 515 nm. A Thorlabs LB1945-A bi-convex  
 145 lens with a 200 mm focal length lens collimates the output beam of our laser light source. The  
 146 collimated beam goes through a wire grid linear polarizer, Thorlabs LPVISE100-A, to maintain a  
 147 polarization aligned with our phase-only Spatial Light Modulator's fast axis (SLM). The linearly  
 148 polarized collimated beam bounces off an anti-reflection coated Pellicle beamsplitter, Thorlabs  
 149 BP245B1, towards our 0.90 degrees tilted phase-only SLM, Holoeye Pluto 2.0 (tilted half order).  
 150 To avoid undiffracted light, we add a horizontal grating to the displayed holograms on our SLM.  
 151 The horizontally grating hologram,  $u'_0$  can be calculated as

$$u'_0(x, y) = \begin{cases} e^{-j(\phi(x, y) + \pi)} & \text{for } x = \text{odd} \\ e^{-j\phi(x, y)} & \text{for } x = \text{even} \end{cases} \quad (6)$$

152 where  $\phi$ , the original phase of  $u_0$ , is modified. This way, we steer the location of the reconstructed  
 153 image in space away from undiffracted light. The tilt angle of our SLM calculated using the

154 diffraction equation formulated as

$$m\lambda = \Delta a \sin(\theta), \quad (7)$$

155 where  $m$  is the half-order (0.5),  $\Delta a$  is pixel pitch of a SLM and the  $\theta$  is the angular location of  
156 the grating plane. For our system,  $\theta$  is calculated as  $1.80^\circ$ . So the required tilt angle  
157 for the SLM is  $\frac{\theta}{2} \approx 0.90^\circ$ . In the rest of the setup, the phase-modulated beam goes through  
158 the Pellicle beamsplitter. In the next stage, the beam passes focusing lenses, a combination  
159 of Thorlabs LA1908-A and LB1056-A. A pinhole aperture, Thorlabs SM1D12, follows the  
160 lenses at the focal distance of the focusing lenses to avoid undiffracted light. We capture the  
161 image reconstructions of our hologram dataset optimized using ideal holographic light transport  
162 from our setup with a lensless image sensor, Point Grey GS3-U3-23S6M-C USB 3.0. For each  
163 captured image reconstruction, we applied homography correction for the captures, so that we  
164 can compare it against a ground-truth image or a simulated reconstruction. The holograms in our  
165 work are always reconstructed for a target image plane at 7 cm away from our proof-of-concept  
166 holographic display.

#### 167 4. Learned holographic light transport

168 We provide sample photographs showing image reconstructions captured from our proof-of-  
169 concept holographic display in Figure 2. These photographs are a result of holograms optimized  
170 using the ideal holographic light transport model. We also provide input holograms and their  
171 simulated results for comparison. The visual mismatch between photographs and simulated  
172 results provides a good understanding of the image quality issues discussed earlier.

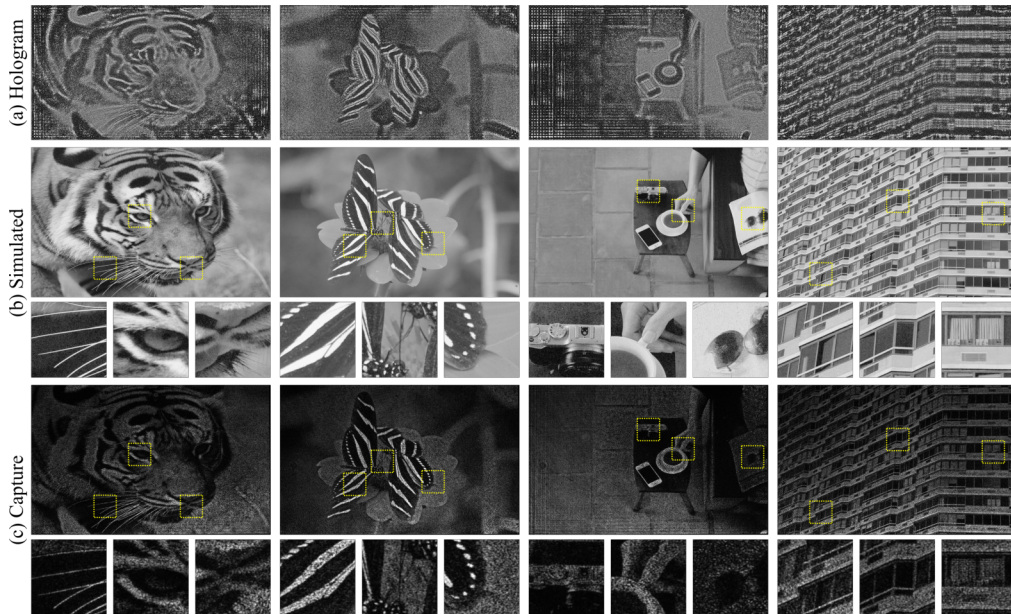


Fig. 2. Mismatch between simulated and experimental results when using ideal holographic light transport. For a given (a) phase-only hologram, A simulated result can provide (b) a perfect image reconstruction, while the same hologram in (c) a real holographic display fail in achieving such image reconstructions as we show in Dataset 1 (Ref. [35]).

173 To combat this mismatch illustrated in Figure 2, we take advantage of our dataset of photographs  
174 from the proof-of-concept prototype and their corresponding optimized holograms that used the



175 ideal holographic light transport model (Dataset 1 [35]). With a Stochastic Gradient Descent  
 176 based optimization method [32, 33] and a learning rate of 0.002, we set to learn a complex kernel,  
 177  $h_l(x, y)$  using the loss function at Equation 5 that will replace the original  $h(x, y)$  from the ideal  
 178 case. This newly optimized  $h_l(x, y)$  can be best described as a transfer function that takes an  
 179 ideal input hologram and provides an image reconstruction similar to the captured photographs  
 180 in our dataset. The code base of our learning process follows the same optimization described  
 181 in Section 2 (refer to [realistic\\_holography:optics L87-L137](#)). The phase and amplitude of the  
 182 learned complex kernel,  $h_l(x, y)$ , and the ideal complex kernel,  $h(x, y)$ , are provided in Figure 3  
 183 for comparison.

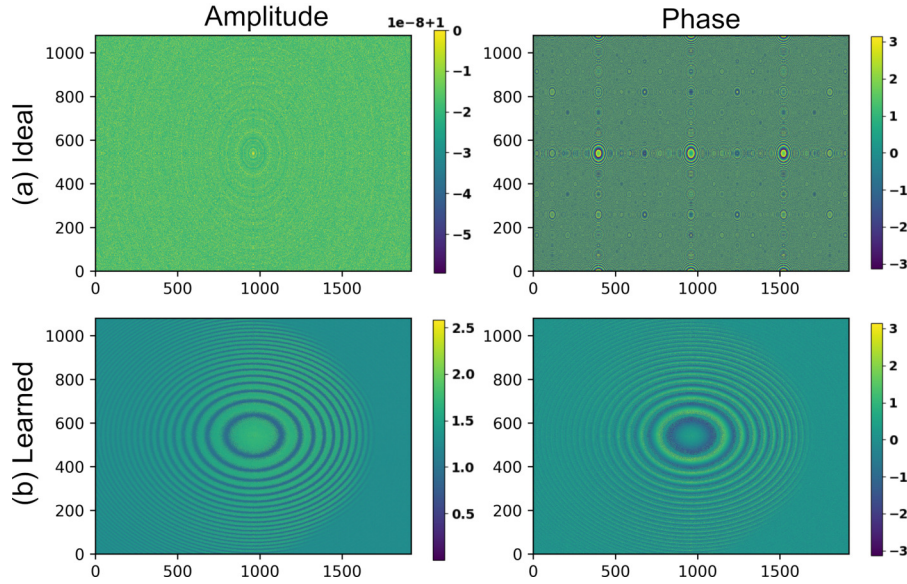


Fig. 3. A phase and amplitude comparison between complex kernels used in (a) ideal holographic light transport and (b) learned holographic light transport.

## 184 5. Evaluation

185 Now that we have a learned transfer function,  $h_l(x, y)$ , shown in Figure 3, we look into how  
 186 this kernel representing the learned holographic light transport can help us to optimize new  
 187 holograms. Assume that the learned kernel is more realistic than the original ideal kernel. In that  
 188 hypothesis, the optimized holograms should lead to image reconstruction results better in terms  
 189 of image quality in the experimental case. Meantime, we should also expect that the mismatch  
 190 between simulations and experiment cases to be mitigated. We challenge these assumptions  
 191 by optimizing holograms using  $h_l(x, y)$  instead of  $h(x, y)$ . In our exploration for optimizing  
 192 holograms using the learned holographic light transport, we rely on the same process described  
 193 in Section 2 (refer to [realistic\\_holography:optics L45-85](#)).

194 **Image quality.** We provided a visual comparison between holograms generated using the ideal  
 195 holographic light transport and learned holographic light transport in Figure 4. The visual  
 196 quality of the reconstructed images in our proof-of-concept holographic display using the learned  
 197 holographic light transport shows a significant improvement over the ideal case. We believe  
 198 this is because imperfections in our proof-of-concept holographic display are accounted for in  
 199 our transfer function. We kindly invite the readers to observe the visual difference between the

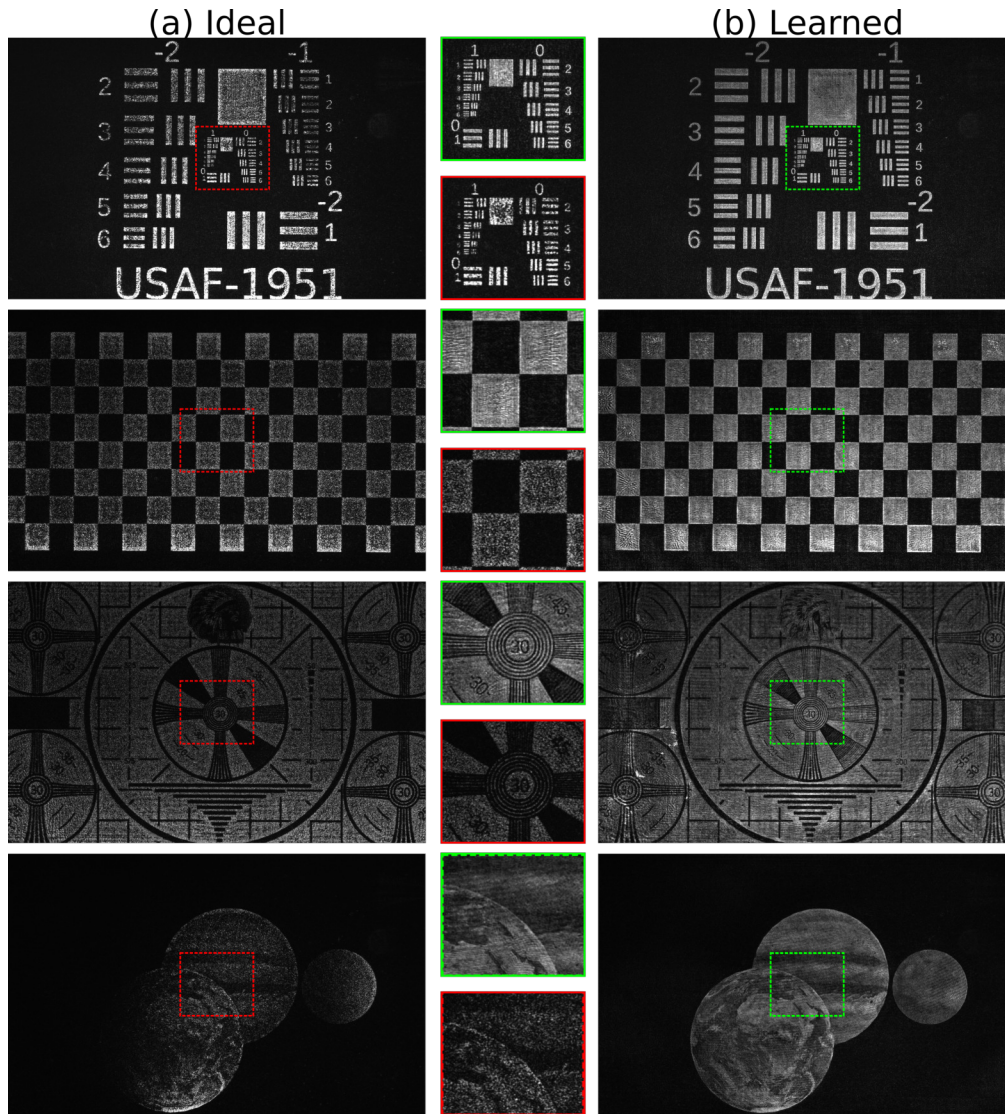


Fig. 4. A visual comparison between (a) ideal holographic light transport and (b) learned holographic light transport in reconstructing images. Both of the photographs are captured with optimized holograms using corresponding holographic light transport models and our proof-of-concept prototype. Note that target image at both cases are not used in our training set (DIV2K [34]).

200 ideal transfer function and the learned transfer function provided in Figure 3. Please note the  
 201 asymmetry in the learned kernel, which does not exist in the case of an ideal kernel.

202 **The mismatch between simulations and experiments.** Our learned holographic light trans-  
 203 port can approximate a transfer function of our proof-of-concept display accurately (Training L2  
 204 loss: 0.0028 and test loss: 0.0034 – learned reconstruction versus captured ground truth images –  
 205 note that images are normalized between zero and one). We compare image reconstructions from  
 206 our simulations with our experimental results from our proof-of-concept holographic display to

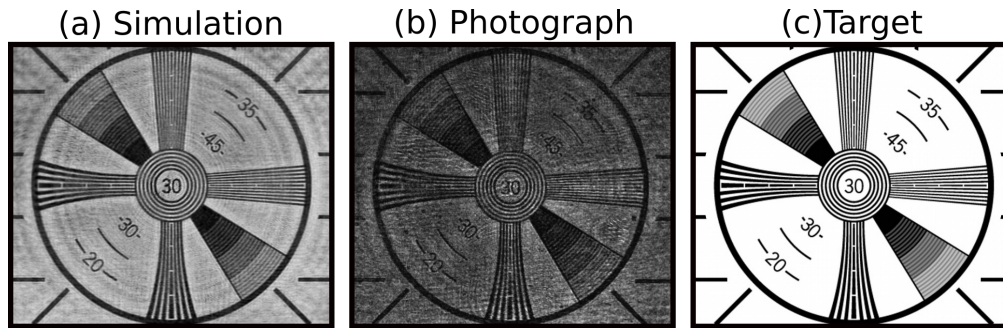


Fig. 5. Learned simulation (a) versus real photograph (b). Ideal light transport based hologram optimization estimates unrealistic results in simulation. On the other hand, for a given target image (c), simulations based on learned holographic light transport closely resembles the experimental results.

207 provide evidence that this is the case. This comparison is sampled in Figure 5. Our simulations'   
 208 brightness and contrast levels with learned holographic light transport do not truly match our   
 209 photographs from our experimentation. However, the spatial content in experimental cases   
 210 resembles the simulated reconstructions closely and even giving us an excellent hint about what   
 211 to expect in terms of visual quality from a given holographic display. If further tweaking is   
 212 needed, the brightness mismatch in the ideal and learned cases can be improved by following a   
 213 manual calibration routine. In the supplementary documentation of work by Choi et al. [36],   
 214 curious readers can find highly detailed documentation on minimizing the average difference   
 215 between simulation and a physical prototype by adjusting laser power and exposure time. We   
 216 have not conducted such a calibration for this work, as we wanted to show the improvement over   
 217 an uncalibrated system.

218 **What did we learn from the learned kernel?** The holographic light transport kernel learned   
 219 within this work (see Figure 3) indicates that the phase and amplitude behaviour of our physical   
 220 light source is not homogenous in terms of angular emission. The readers may observe this fact by   
 221 carefully checking the asymmetry of the kernel in Figure 3. The amplitude values are far greater   
 222 than the ideal kernel, thus suggesting that to get to brighter images, the hologram optimization   
 223 has to consider this correlation. This fact can be observed in Figure 4 as the dynamic range,   
 224 and brightness levels are better preserved in the learned method. Note that the learned kernel is   
 225 the point-spread function of the given holographic display. Thus, resolution characteristics of   
 226 the holographic display can also be analyzed in the future by studying the limits of a learned   
 227 point-spread function. Finally, note that a single kernel can only capture a global mean of a   
 228 general trend in a holographic display. We will discuss how to improve our learned method in   
 229 the future in the final paragraph of this section.

230 **Comparison with the state of the art.** The leading state-of-the-art methods [5,6] that bridge   
 231 the gap between simulations and physical holographic displays consists of convolutional neural   
 232 networks. Specifically, the work by Peng et al. [5] relies on more than eight million parameters   
 233 to tune in a training process of neural networks. Many parameters and layers are needed to   
 234 efficiently realize the correlation between a hologram and a final reconstructed image. Otherwise,   
 235 the connections between the pixels of a hologram and a final reconstructed image may not be   
 236 fully identified (locality issue). This locality issue arises from the fact that such models use small   
 237 kernel sizes. In contrast, our work decreases this number of tunable parameters to half, four   
 238 million parameters (2x1080x1920 – amplitude and phase), while relying on kernel sizes that is



239 the same as an input image which avoids locality issue. The work by Maimone et al. [37] uses  
240 one-dimensional separable functions for reducing the memory footprint in classical CGH [37]  
241 for ideal complex forms such as quadratic phase functions. Drawing inspiration from that work,  
242 we speculate that further reduction may be possible by storing a parametric form of a learned  
243 complex kernel.

244 The readers of our work may ask if our approach is the solution that could provide the most  
245 remarkable accuracy in bridging the gap between simulations and experiments in holography.  
246 We followed a similar approach to the classical model, where a single convolutional kernel  
247 formulates the transfer function of light transport. Hence, our approach is accurate as long as  
248 a single kernel is reliable to describe the light transport. To improve accuracy further and to  
249 have one-to-one matching simulations in the future, we speculate that approaches with spatially  
250 varying convolutional kernels can provide more capacity to accommodate for a genuinely realistic  
251 simulation. On the other hand, we learn the light transport between a hologram and an image  
252 plane. Approaches that provide three-dimensional image reconstructions in CGH require a  
253 transfer function representing the relationship between a single hologram and multiple image  
254 planes. In our approach, we have to learn the kernel for each plane using a set of images. In the  
255 future, a complete form of our approach can potentially be derived where a data set with diverse  
256 image reconstruction distances helping to learn a parametric light transport rather than per plane  
257 learning. Our work does an excellent job in capturing optical aberrations and imperfections of a  
258 holographic display. Our work can be best described as the simplest form of improving realism  
259 in CGH algorithms without dealing with complex experimentation or complex algorithmic  
260 approaches.

## 261 6. Conclusion

262 Holographic displays often require tedious effort to optimize holograms for the best possible  
263 image quality. We propose a new learned method to address this issue with holographic displays in  
264 a simple way. The core of our approach is in a learning procedure that allows one to approximate  
265 an accurate holographic light propagation model for a given actual holographic display. With this  
266 approach, we can optimize holograms that can dramatically improve image quality concerning a  
267 typical ideal holographic light transport model. Our method, in turn, enables a simple yet effective  
268 method that does not suffer from the overhead of deriving complex algorithmic approaches while  
269 paving the way towards physically informed learning approaches in the holography domain.

270 **Acknowledgments.** The authors thank the anonymous reviewers for their useful feedback. The authors  
271 also thank Oliver Kingshott and Duygu Ceylan for the fruitful and inspiring discussions improving the  
272 outcome of this research, and Selim Ölçer for helping with the fiber alignment of laser light source in the  
273 proof-of-concept display prototype.

274 **Disclosures.** The authors declare no conflicts of interest.

275 **Data Availability Statement.** The code base discussed in Section 2 and 4 is readily available in the  
276 [Github:complight/realistic\\_holography](https://github.com/complight/realistic_holography). The generated dataset of this work is also available in the [Dataset:](#)  
277 [Phase-only holograms and photographs](#).

## 278 References

- 279 1. J. Orlosky, M. Sra, K. Bektaş, H. Peng, J. Kim, N. Kos' myna, T. Hollerer, A. Steed, K. Kiyokawa, and K. Akşit,  
280 "Telelife: The future of remote living," arXiv preprint arXiv:2107.02965 (2021).
- 281 2. G. A. Koulteris, K. Akşit, M. Stengel, R. K. Mantiuk, K. Mania, and C. Richardt, "Near-eye display and tracking  
282 technologies for virtual and augmented reality," in *Computer Graphics Forum*, vol. 38 (Wiley Online Library, 2019),  
283 pp. 493–519.
- 284 3. G.-z. Yang, B.-z. Dong, B.-y. Gu, J.-y. Zhuang, and O. K. Ersoy, "Gerchberg–saxton and yang–gu algorithms for  
285 phase retrieval in a nonunitary transform system: a comparison," *Appl. optics* **33**, 209–218 (1994).
- 286 4. C. Chen, B. Lee, N.-N. Li, M. Chae, D. Wang, Q.-H. Wang, and B. Lee, "Multi-depth hologram generation using  
287 stochastic gradient descent algorithm with complex loss function," *Opt. Express* **29**, 15089–15103 (2021).

- 288 5. Y. Peng, S. Choi, N. Padmanaban, and G. Wetzstein, "Neural holography with camera-in-the-loop training," *ACM*  
289 *Transactions on Graph. (TOG)* **39**, 1–14 (2020).
- 290 6. P. Chakravarthula, E. Tseng, T. Srivastava, H. Fuchs, and F. Heide, "Learned hardware-in-the-loop phase retrieval for  
291 holographic near-eye displays," *ACM Transactions on Graph. (TOG)* **39**, 1–18 (2020).
- 292 7. R. Li and L. Cao, "Progress in phase calibration for liquid crystal spatial light modulators," *Appl. Sci.* **9**, 2012 (2019).
- 293 8. J. Wu, K. Liu, X. Sui, and L. Cao, "High-speed computer-generated holography using an autoencoder-based deep  
294 neural network," *Opt. Lett.* **46**, 2908–2911 (2021).
- 295 9. T. Zhao, J. Liu, X. Duan, Q. Gao, J. Duan, X. Li, Y. Wang, W. Wu, and R. Zhang, "Multi-region phase calibration of  
296 liquid crystal slm for holographic display," *Appl. optics* **56**, 6168–6174 (2017).
- 297 10. B. Zhang, Y. Chen, and R. Feng, "A calibration method for phase-only spatial light modulator," in *2017 Progress In*  
298 *Electromagnetics Research Symposium-Spring (PIERS)*, (IEEE, 2017), pp. 133–135.
- 299 11. G. Krasin, N. Stsepuro, I. Gritsenko, and M. Kovalev, "Holographic method for precise measurement of wavefront  
300 aberrations," in *Holography: Advances and Modern Trends VII*, vol. 11774 (International Society for Optics and  
301 Photonics, 2021), p. 1177407.
- 302 12. X. Xun and R. W. Cohn, "Phase calibration of spatially nonuniform spatial light modulators," *Appl. optics* **43**,  
303 6400–6406 (2004).
- 304 13. J. Vorba, O. Karlík, M. Šik, T. Ritschel, and J. Křivánek, "On-line learning of parametric mixture models for light  
305 transport simulation," *ACM Transactions on Graph. (TOG)* **33**, 1–11 (2014).
- 306 14. M. Ayoub, "A review on light transport algorithms and simulation tools to model daylighting inside buildings," *Sol.*  
307 *Energy* **198**, 623–642 (2020).
- 308 15. J. Jönsson and E. Berrocal, "Multi-scattering software: part i: online accelerated monte carlo simulation of light  
309 transport through scattering media," *Opt. Express* **28**, 37612–37638 (2020).
- 310 16. S. A. Reza, M. La Manna, S. Bauer, and A. Velten, "Phasor field waves: A Huygens-like light transport model for  
311 non-line-of-sight imaging applications," *Opt. express* **27**, 29380–29400 (2019).
- 312 17. T. Rittig, D. Sumin, V. Babaei, P. Didyk, A. Voloboy, A. Wilkie, B. Bickel, K. Myszkowski, T. Weyrich, and  
313 J. Křivánek, "Neural acceleration of scattering-aware color 3d printing," in *Computer Graphics Forum*, vol. 40  
314 (Wiley Online Library, 2021), pp. 205–219.
- 315 18. G. Corbellini, K. Aksit, S. Schmid, S. Mangold, and T. R. Gross, "Connecting networks of toys and smartphones  
316 with visible light communication," *IEEE Commun. Mag.* **52**, 72–78 (2014).
- 317 19. C. Jang, O. Mercier, K. Bang, G. Li, Y. Zhao, and D. Lanman, "Design and fabrication of freeform holographic  
318 optical elements," *ACM Transactions on Graph. (TOG)* **39**, 1–15 (2020).
- 319 20. K. Akşit, "Patch scanning displays: spatiotemporal enhancement for displays," *Opt. express* **28**, 2107–2121 (2020).
- 320 21. P. Chakravarthula, D. Dunn, K. Akşit, and H. Fuchs, "Focusar: Auto-focus augmented reality eyeglasses for both real  
321 world and virtual imagery," *IEEE transactions on visualization computer graphics* **24**, 2906–2916 (2018).
- 322 22. R. Li, E. Whitmire, M. Stengel, B. Boudaoud, J. Kautz, D. Luebke, S. Patel, and K. Akşit, "Optical gaze tracking with  
323 spatially-sparse single-pixel detectors," in *2020 IEEE International Symposium on Mixed and Augmented Reality*  
324 *(ISMAR)*, (IEEE, 2020), pp. 117–126.
- 325 23. G. Aydındoğan, K. Kavaklı, A. Şahin, P. Artal, and H. Ürey, "Applications of augmented reality in ophthalmology,"  
326 *Biomed. optics express* **12**, 511–538 (2021).
- 327 24. J. C. Heurtley, "Scalar rayleigh–sommerfeld and kirchhoff diffraction integrals: a comparison of exact evaluations for  
328 axial points," *JOSA* **63**, 1003–1008 (1973).
- 329 25. J. W. Goodman, "Introduction to fourier optics, roberts & co," Publ. Englewood, Colo. (2005).
- 330 26. K. Matsushima and T. Shimobaba, "Band-limited angular spectrum method for numerical simulation of free-space  
331 propagation in far and near fields," *Opt. express* **17**, 19662–19673 (2009).
- 332 27. W. Zhang, H. Zhang, and G. Jin, "Band-extended angular spectrum method for accurate diffraction calculation in a  
333 wide propagation range," *Opt. Lett.* **45**, 1543–1546 (2020).
- 334 28. W. Zhang, H. Zhang, and G. Jin, "Adaptive-sampling angular spectrum method with full utilization of space-bandwidth  
335 product," *Opt. Lett.* **45**, 4416–4419 (2020).
- 336 29. M. Sypek, "Light propagation in the fresnel region. new numerical approach," *Opt. communications* **116**, 43–48  
337 (1995).
- 338 30. K. Akşit, A. S. Karadeniz, P. Chakravarthula, W. Yujie, K. Kavaklı, Y. Itoh, and D. R. Walton, "Odak 0.1.9,"  
339 <https://doi.org/10.5281/zenodo.5526684> (2021).
- 340 31. A. Paszke, S. Gross, S. Chintala, G. Chanan, E. Yang, Z. DeVito, Z. Lin, A. Desmaison, L. Antiga, and A. Lerer,  
341 "Automatic differentiation in pytorch," in *NIPS 2017 Workshop on Autodiff.* (2017).
- 342 32. D. P. Kingma and J. Ba, "Adam: A method for stochastic optimization," arXiv preprint arXiv:1412.6980 (2014).
- 343 33. I. Loshchilov and F. Hutter, "Decoupled weight decay regularization," arXiv preprint arXiv:1711.05101 (2017).
- 344 34. A. Ignatov, R. Timofte, T. V. Vu, T. M. Luu, T. X. Pham, C. V. Nguyen, Y. Kim, J.-S. Choi, M. Kim, J. Huang, J. Ran,  
345 C. Xing, X. Zhou, P. Zhu, M. Geng, Y. Li, E. Agustsson, S. Gu, L. V. Gool, E. de Stoutz, N. Kobyshev, K. Nie,  
346 Y. Zhao, G. Li, T. Tong, Q. Gao, L. Hanwen, P. N. Michelini, Z. Dan, H. Fengshuo, Z. Hui, X. Wang, L. Deng,  
347 R. Meng, J. Qin, Y. Shi, W. Wen, L. Lin, R. Feng, S. Wu, C. Dong, Y. Qiao, S. Vasu, N. T. Madam, P. Kandula, A. N.  
348 Rajagopalan, J. Liu, and C. Jung, "Pirm challenge on perceptual image enhancement on smartphones: report," in  
349 *European Conference on Computer Vision (ECCV) Workshops*, (2019).
- 350 35. K. Kavaklı, H. Ürey, and K. Akşit, "Phase-only holograms and captured photographs," (2021).

- 351 36. S. Choi, J. Kim, Y. Peng, and G. Wetzstein, "Optimizing image quality for holographic near-eye displays with  
352 michelson holography," *Optica* **8**, 143–146 (2021).
- 353 37. A. Maimone, A. Georgiou, and J. S. Kollin, "Holographic near-eye displays for virtual and augmented reality," *ACM*  
354 *Transactions on Graph. (Tog)* **36**, 1–16 (2017).